https://doi.org/10.5194/egusphere-2026-4265
Preprint. Discussion started: 24 August 2026

Tropical cyclone amplifies anthropogenic influences on aerosol-cloud interactions over the South China Sea

Hengjia Ou[1,2], Mingfu Cai[3], Haichao Wang[1], Xue Ni[4], Shixin Mai[1], Qibin Sun[5], Baoling Liang[6], Kunpeng Chen[7], Tao Deng[2], Sun Jiaren[3], Shengzhen Zhou[1], and Jun Zhao[1,†]

[1] School of Atmospheric Sciences, Sun Yat-sen University, and Southern Marine Science and Engineering Guangdong Laboratory (Zhuhai), Zhuhai 519082, China

[2] Institute of Tropical and Marine Meteorology, China Meteorological Administration, Guangzhou 510640, China

[3] Guangdong Province Engineering Laboratory for Air Pollution Control, Guangdong Provincial Key Laboratory of Water and Air Pollution Control, South China Institute of Environmental Sciences, MEE, Guangzhou 510655, China

[4] Guangzhou Ecological and Agricultural Meteorological Center, Guangzhou 511430, China

[5] Guangzhou Sub-branch of Guangdong Ecological and Environmental Monitoring Center, Guangzhou 510006, China

[6] Dongguan Meteorological Bureau, Dongguan 523086, China

[7] State Key Laboratory of Regional Environment and Sustainability, School of Environment, Tsinghua University, Beijing 100084, China

[†] Deceased, 10/2024

Correspondence to: Mingfu Cai (mingfu0721@hotmail.com) and Haichao Wang (wanghch27@mail.sysu.edu.cn)

https://doi.org/10.5194/egusphere-2026-4265
Preprint. Discussion started: 24 August 2026

Abstract. Tropical cyclones can influence marine aerosol-cloud interactions by transporting continental anthropogenic pollutants over the ocean. However, this process and its impact remain poorly understood due to lack of direct measurements. Using shipborne measurements over the South China Sea (SCS) from 22 June to 5 July 2022, we investigated how a typical TC Chaba altered aerosol physicochemical properties and cloud microphysical responses. As TC Chaba developed, its circulation altered regional transport pathways, shifting air masses from local marine origin to long-range transport from the Indochina Peninsula and causing pronounced increases in non-refractory submicron particulate matter ($NR\text{-}PM_1$) concentrations. Organic aerosol (OA) increased from 14.6% to 44.9% of $NR\text{-}PM_1$ after the influence of TC Chaba, mainly due to enhanced oxygenated OA (OOA) from long-range transport together with enhanced local heterogeneous oxidation, as indicated by the higher OA oxidation state and increasing OOA concentrations with O*x* and relative humidity. These changes led to a ~60% decrease in aerosol hygroscopicity (κ), while an ~27% increase in κ_{OA}, which outweighed the modest particle size increase and resulted in a lower bulk activation ratio. Furthermore, CCN concentrations increased by up to sixfold because of enhanced aerosol concentrations. Combined observations and cloud parcel simulations indicate that the aerosol perturbations decreased cloud droplet effective radius by 11-37% and increased the autoconversion radius by 6-26%, enhancing cloud reflectivity and suppressing warm-rain formation. Satellite observations further confirmed smaller cloud droplets. These results demonstrate a strong TC influence on marine cloud microphysics and radiative effects.

https://doi.org/10.5194/egusphere-2026-4265
Preprint. Discussion started: 24 August 2026

1. Introduction

Marine aerosols play an important role in the Earth's radiation budget and climate system (Chen et al., 2014; Ipcc, 2021). However, substantial uncertainties remain in quantifying their radiative effects, largely due to their indirect influence on clouds (Wall et al., 2023; Qiu et al., 2024; Lu and Seinfeld, 2005). By acting as cloud condensation nuclei (CCN), marine aerosols affect cloud formation, lifetime, and albedo, yet these processes are still difficult to constrain in climate models (Wang et al., 2011; Boucher and Lohmann, 1995). In the remote marine boundary layer (MBL), natural aerosols, like sea salt aerosols, often dominate the CCN population (Kristensen et al., 2016; King et al., 2012). In contrast, marginal seas near continental outflow are frequently influenced by anthropogenic emissions and biomass burning plumes, creating mixed air masses with both marine and continental characteristics (Liu et al., 2013; Qin et al., 2024). This mixture increases aerosol loading and alters particle composition and hygroscopicity, thereby modifying CCN activity-which means the ability of aerosols to serve as CCN-and introducing considerable uncertainty into regional aerosol–cloud interaction (ACI) assessments (Jose et al., 2020). Model ensemble experiments reveal that uncertainties in marine aerosol parameterizations, cause global mean radiative forcing variations of about ±0.3–0.4 W m^{-2} (Bhatti et al., 2026). Observational constraints further suggest that reducing these parameterization uncertainties may decrease radiative forcing uncertainty by up to 20% (Regayre et al., 2020). These findings underscore that variations in aerosol physicochemical properties are a key driver of ACI uncertainty, particularly over marine environments.

The South China Sea (SCS) is a typical marginal sea, surrounded by regions with substantial anthropogenic influence including southern China, the Indochina Peninsula, the Philippine Archipelago, and the Malay Peninsula—which makes it particularly sensitive to continental outflow and the long-range transport of air pollutants (Cai et al., 2020; Ou et al., 2025). The region is also frequently traversed by tropical cyclones (TCs) (Wang et al., 2007; Wang et al., 2014). TCs influence atmospheric aerosols over the SCS through two main pathways: (1) TC-related precipitation effectively scavenges airborne particles (Lin and Huang, 2025; Chen et al., 2010); (2) the strong TC-induced circulation significantly modifies regional airflow, leading to shifts in the air masses reaching the SCS, and altering the physicochemical properties of aerosols consequently(Liang et al., 2021). Furthermore, TC-driven changes in aerosol properties can modulate cloud formation and precipitation processes, which in turn

https://doi.org/10.5194/egusphere-2026-4265
Preprint. Discussion started: 24 August 2026

may affect TC intensity and lifetime (Wang et al., 2023; Wang et al., 2014). However, quantifying the combined impacts of these TC-driven processes on aerosol physicochemical properties and subsequent cloud formation in the marine boundary layer (MBL) remains a major observational challenge.

Current understanding largely relies on satellite products, model simulations, and sparse land-based observations, which cannot resolve the rapid in situ changes within the MBL during and after TC passage. Previous satellite and modeling studies suggest that anthropogenic emissions may increase the occurrence of nearshore TCs and intensify TC-related precipitation, while suppressing TC strength and slowing development (Wang et al., 2014; Wang et al., 2023). Coastal measurements have also shown that TCs can worsen ozone and $PM_{2.5}$ pollution in the Southern China (Shao et al., 2022; Wang et al., 2022). However, observational evidence over the ocean is still lacking, particularly regarding how TCs modify aerosol physicochemical properties and cloud microphysical processes. Closing this gap is essential for understanding the effects of TCs on ACI and their implications for regional climate.

In this study, a comprehensive shipborne observation campaign was conducted over the SCS, which captured the complete life cycle of TC Chaba. These unique measurements allow us to systematically examine how TC-driven alterations in atmospheric circulation reshape aerosol physicochemical properties, modulate CCN activities, and ultimately influence cloud microphysical processes in the marine boundary layer.

2. Method

2.1 Cruise information

A 15-day shipboard measurement was conducted from 20 June to 5 July 2022 in the SCS aboard the "Sun Yat-sen University" vessel, during the active summer monsoon period when the region was predominantly influenced by the southwest monsoon (Fig. S1). The vessel departed from Gaolan Port (Zhuhai), traveled to the vicinity of the Xisha Islands, and primarily operated—while also performing TC-avoidance maneuvers—in the waters south of Hainan Island and east of Vietnam, before returning to Gaolan Port (Fig. 1j). All instruments were put in a chamber in temperature-controlled chamber. The sample line was from the window of chamber to the driving room which is about 20 m from sea surface level. During the shipborne campaign, the observations covered the full life cycle of a TC event. TC

https://doi.org/10.5194/egusphere-2026-4265
Preprint. Discussion started: 24 August 2026

Chaba began to influence the circulation over the SCS around 28 June, was officially named by the China Meteorological Administration on 29 June and was removed from the naming list on 4 July (Figs.1c-i). Based on the above information, the period from June 22 to 27 is defined as the pre–TC period, and the period from June 28 to July 4 is defined as the post–TC Chaba period in this study.

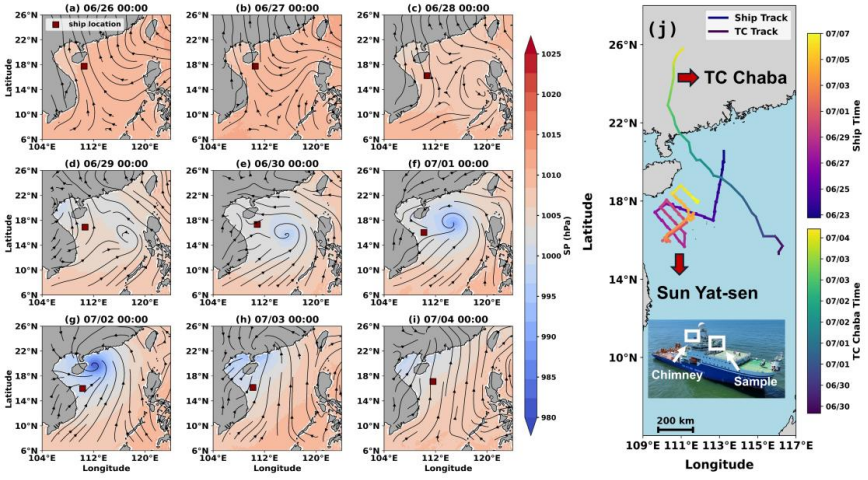

Figure 1. Changes in surface pressure (SP) and wind fields over the South China Sea before and after the formation of Tropical Cyclone (TC) Chaba (26 June–4 July, a-i). The cruise track of "Sun Yat-sen" research vessel, the sampling locations, the ship exhaust stack position, and the track of TC Chaba.

2.2 Instruments

The chemical composition of non-refractory submicron particulate matter (NR-PM_1), including sulfate, nitrate, organics, ammonium, and chloride, was measured using a time-of-flight aerosol chemical speciation monitor with a standard vaporizer (SV-ToF-ACSM; Aerodyne Inc., USA). The instrument operated with a time resolution of ~10 min. Ionization efficiency (IE) and relative ionization efficiency (RIE) were calibrated using ammonium nitrate (NH_4NO_3) and ammonium sulfate ($(NH_4)_2SO_4$) before and after each campaign. The nitrate IE values were 112.4 ions pg^{-1}. The RIE values for ammonium were 3.43, while those for sulfate were 0.77. The collection efficiency (CE) was 0.5. Assuming an average aerosol density of 1.5 g cm^{-3} (Geller et al., 2006), the mass concentrations from the SMPS and ToF-ACSM showed strong correlations, with coefficients of 0.84 (Fig. S2).

Size-resolved CCN activity was measured using the scanning mobility CCN analysis (SMCA) method proposed by Moore et al. (2010). The setup consisted of a scanning mobility particle sizer (SMPS)

https://doi.org/10.5194/egusphere-2026-4265
Preprint. Discussion started: 24 August 2026

coupled with a cloud condensation nuclei counter (CCNc; CCNc-200, DMT Inc., USA) (Fig. S3). The SMPS included a differential mobility analyzer (DMA; model 3082, TSI Inc.) and a condensation particle counter (CPC; model 3756, TSI Inc.). The SMPS and CCNc were used to measure particle number size distributions (PNSD) and size-resolved CCN number concentrations across mobility diameters of 12–593 nm. The detail setting was described in the Text S1.

Before each campaign, the CCNc was calibrated at every SS using $(NH_4)_2SO_4$ particles. A detailed description of the calibration and instrument configuration is provided in Cai et al., 2018.Cai et al. (2018) The overall uncertainty of the size-resolved particle number concentration measured by the system is approximately 5%–6%.(Moore et al., 2010)

The trace gases (NO, NO_2, O_3, and SO_2) were measured by gas analyzers (TELEDYNE API Inc.), which were calibrated with standard gases before the measurement. The timeseries of trace gases was shown in Fig. S4.

To ensure the reliability of atmospheric measurements over the SCS and to minimize contamination from ship emissions, data quality controls were conducted, which was detailed in Text S2. 90.1% of the data (10-minute resolution) were classified as clean and retained for subsequent analysis.

2.3 Data analysis

In this study, PMF was applied to the organic aerosol (OA) mass spectra measured by the SV-ToF-ACSM which was described detailly in Text S3; thus, the analysis is referred to as OA PMF. Diagnostic plots used to evaluate the PMF solution are shown in Fig. S5. Three OA factors were resolved, including two primary OA factors—hydrocarbon-like OA (HOA) and biomass-burning OA (BBOA)—and one secondary OA factor, oxygenated OA (OOA) (Fig. S6). OOA constituted the largest fraction of OA, accounting for 82.6% (Fig. S7a). Its oxidation indicator, the fraction of m/z 44 (CO_2^+, f_{44}), was 0.31—similar to the f_{44} value of LVOOA (0.31) observed over the SCS in 2018 (Liang et al., 2021), and slightly lower than that of OOA (0.33) measured in 2019 (Fig. S7b) (Sun et al., 2023). HOA was the second largest contributor (15.6%). Its mass spectrum is characterized by prominent C_nH_{2n-1} and C_nH_{2n+1} ion series (e.g., m/z 41, 43, 55, 57, 69, and 71) (Fig. S6a1), consistent with the mean HOA profile reported by Ng et al., 2011.Ng et al. (2011) In contrast, BBOA accounted for only a small fraction (1.7%), and its spectrum did not fully resemble typical BBOA profiles (Fig. S6b1). Nonetheless, its enhanced m/z 60

https://doi.org/10.5194/egusphere-2026-4265
Preprint. Discussion started: 24 August 2026

signal—the most characteristic marker of BBOA—supports its identification as BBOA. The m/z 60 ion corresponds primarily to $C_2H_4O_2^+$, a pyrolysis product of levoglucosan and related compounds, and is a direct tracer of cellulose/hemicellulose combustion. Therefore, this factor is interpreted as BBOA in this study.

The size-resolved number concentrations of total particles and CCN were obtained from the SMPS and CCNc using the SMCA method. The activation diameter was derived by fitting the activation ratio (AR = N_{CCN}/N_{CN}) as a function of dry particle diameter at each SS using the following sigmoid function:

$$AR = \frac{B}{1+\left(\frac{D_P}{D_{50}}\right)^C} \quad (1)$$

where AR is the size-resolved AR, D_P indicates dry particle diameter (nm); B, C, and D_{50} are the three fitting parameters, representing the asymptote, the slope, and the inflection point of the sigmoid, respectively.(Moore et al., 2010) The parameter D_{50}, also referred to as the critical diameter, corresponds to the particle size at which 50% of particles activate at a given SS. The SMCA fitting results obtained in this study are shown in Fig. S8.

The hygroscopicity parameter κ, which characterizes CCN activity within the κ-Köhler theory, was calculated following:Petters and Kreidenweis (2007)

$$\kappa = \frac{4A^3}{27{D_{50}}^3(lnS_c)^2}, A = \frac{4\sigma_{s/a}M_w}{RT\rho_w} \quad (2)$$

where ρ_w is the density of pure water which value is about 997.04 kg m^{-3} at 298.15 K, M_W is the molecular weight of water which value is 0.018 kg mol^{-1}, $\sigma_{s/a}$ represents the surface tension of the solution-air interface and is assumed to be equal to the surface tension of pure water ($\sigma_{s/a}$=0.0728 N m^{-1} at 298.15 K), R is the universal gas constant (8.314 J mol^{-1} K^{-1}), and T denotes thermodynamic temperature in kelvin, which is 298.15 K in this study. Additionally, it is noting that the estimated κ values refer to particles with the D_{50}.

Due to the malfunction of column B, the N_{CCN} was derived from size-resolved AR at a given SS obtained using the SMCA method, together with the measured N_{CN}. N_{CCN} was calculated following,Cai et al. (2018) using the equation:

$$N_{CCN}(SS) = \int_0^\infty AR(SS, D_P)N_{CN}(D_P)dD_p \quad (3)$$

where N_{CCN}(SS) is the CCN number concentration at a specific SS, AR(SS, D_p) is the ratio of N_{CCN} at a specific SS to N_{CN} on a specific diameter from the SMCA method and $N_{CN}(D_P)$ is the particle number

https://doi.org/10.5194/egusphere-2026-4265
Preprint. Discussion started: 24 August 2026

concentration at a specific diameter (D_P). Because direct measurements of total N_{CCN} were unavailable, the values derived from Eq. (3) are treated as the observed CCN number concentrations ($N_{CCN,obs}$) in this study. Previous studies have demonstrated that this approach—estimating size-resolved CCN using a single column of the CCNc-200—yields result that closely match those obtained from direct measurements using the other column of the instrument.(Lathem and Nenes, 2011; Meng et al., 2014) These findings support the robustness and reliability of the method.

After obtaining the value of $N_{CCN,obs}$, the bulk AR can be calculated as follows:

$$\text{bulk AR(SS)} = \frac{N_{CCN,obs}(\text{SS})}{N_{CN,tot}} \quad (4)$$

where the $N_{CN,tot}$ represents the total particle number concentration.

To integrate our observations and further investigate how variations in aerosol physicochemical properties influence cloud microphysics, we used the 0-D cloud parcel model Pyrcel to simulate aerosol activation into cloud droplets at cloud base. Based on these simulations, we quantified the impact of changes in cloud droplet number concentration (N_C) on cloud microphysical properties during pre-TC Chaba and post-TC Chaba periods. The Pyrcel model describes the growth and evolution of cloud droplet size distributions from a prescribed aerosol population. The model was initialized with aerosol particle size distributions for the Aitken and accumulation modes observed during pre-TC Chaba and post-TC Chaba periods (Fig. S9). κ at 0.7% SS and 0.4% SS were assumed to represent hygroscopicity of the Aitken and accumulation modes, respectively. Meteorological inputs, including average temperature, pressure, and relative humidity, were also prescribed for the pre- and post-Chaba periods.

In the Pyrcel simulations, updraft velocity (w) is a key input parameter that determines the maximum supersaturation. Because w cannot be directly measured, a range of 0.1-2 m s^{-1} was prescribed, representing typical updraft conditions at distances of approximately 400–500 km from the TC center.(Black et al., 1996) It is noted that the minimum distances between our ship location and center of TC Chaba were 400-500 km. Under the actual meteorological conditions and assuming adiabatic ascent, the corresponding SS at cloud base ranged from 0.03% to 0.23% across this w. The detailed input parameters and simulation results were presented in Table S1 and S2, respectively. range. Based on the Pyrcel simulation, the following equations were used to quantify two key ACI effects—the Twomey effect and the Albrecht effect—using the cloud droplet effective radius (r_e) and the critical autoconversion

https://doi.org/10.5194/egusphere-2026-4265
Preprint. Discussion started: 24 August 2026

radius (r_e).

r_e can be calculated as follows:

$$r_e = \beta \left(\frac{3q}{4\pi\rho_w N_c}\right)^{1/3} \quad (5)$$

Here, β is a scaling factor, ρ_w is water density, and N_C is cloud droplet concentration from Pyrcel simulation. Previous studies have analyzed the factors affecting β and proposed corresponding parameterizations (Liu et al., 2008; Rotstayn and Liu, 2009). The liquid water content (LWC), q, is given by:

$$q = \int_0^\infty \frac{4}{3}\pi r^3 \rho_w n(r) dr \quad (6)$$

where n(r) is the cloud droplet number size distribution. Because droplet size distributions were not directly measured in this study, a gamma distribution was assumed, expressed as $n(r) = N_0 r^\mu \exp(-\lambda r)$, where r is the droplet radius, N_0 is the intercept parameter, μ is the shape parameter, and λ is the slope parameter. Typical Gamma-distribution parameters for marine environment are $N_0=8\times10^{-30}$, μ=4, and λ=2×10^{-5} (Miles et al., 2000; Seifert and Beheng, 2006).

To isolate the influence of N_C on r_e, β was assumed to be constant. This assumption is commonly adopted in climate models to reduce uncertainties in other parameters and simplify the analysis (Quaas et al., 2004).

The r_c is parameterized as (Liu et al., 2006):

$$r_c \approx 4.09 \times 10^{-4} \beta^{1/6} \frac{N_c^{1/6}}{q^{1/3}} \quad (7)$$

where β=1.15×10^{23} is an empirical constant. Based on the estimated critical radius, this study further evaluates the impact of anthropogenic influences on the Albrecht effect.

To validate our computational results, we acquired the Cloud particle size liquid data from the MCD06COSP_D3_MODIS product for comparison.(Webb et al., 2017) Since the SCS is located in the subtropics and tropics and our observations were conducted within the boundary layer, we specifically focused on the particle size of low-altitude liquid warm clouds, excluding ice clouds. We defined a study area between 12° and 18° latitude and 109° and 112° longitude (which encompassed the ship's position). Within this region, we calculated the average Cloud particle size liquid values for pre-TC Chaba period and post-TC Chaba period. The MCD06COSP_D3_MODIS product provides daily averaged values, and

https://doi.org/10.5194/egusphere-2026-4265
Preprint. Discussion started: 24 August 2026

examples representing these two periods and calculation range are presented in Fig. S10.

Backward trajectory calculations were conducted using MeteoInfo, an open-source atmospheric analysis package (Wang, 2014), to identify potential source regions. Weekly GDAS1 (Global Data Assimilation System, 1° resolution) meteorological fields were obtained from the NOAA Air Resources Laboratory (ARL) (https://www.ready.noaa.gov/gdas1.php). Backward trajectories were computed every hour for the ship location, producing 72-hour trajectories at an arrival height of 500 m.

3. Result

3.1 Overview

The timeseries of aerosol size distribution, meteorological parameters (RH, T, precipitation, and pressure), CCN number concentration (N_{CCN}) at different SS, and κ were shown in Fig. 2.

Compared to the pre–TC Chaba period, aerosol concentrations increased substantially during the post–TC period, accompanied by pronounced shifts in their physicochemical properties, which are described in detail in the following section. Meteorological conditions also changed notably during this period. Air temperature (T) decreased slightly, with the daytime maximum dropping from ~35 °C during the pre-TC period to ~24 °C during the post-TC period (Fig. 2b). Relative humidity (RH) increased gradually, reaching nearly 100% on 1 July during the post-TC period, coinciding with the only rainfall event observed (Fig. 2b). Atmospheric pressure (P) also declined from ~1005 hPa to below 1000 hPa during the transition from the pre–TC to post-TC period and then gradually recovered to around 1000 hPa as the system weakened (Fig. 2c).The average aerosol particle number concentration (N_{CN}) was 4345 cm^{-3}, slightly higher than the values measured over the SCS in 2014 (~1356 cm^{-3}) and 2018 (~3400 cm^{-3}) but lower than those reported in 2021 (6966 cm^{-3}) (Atwood et al., 2017; Cai et al., 2020; Ou et al., 2025). In contrast to the 2014 and 2021 measurements—both dominated by Aitken-mode particles—the present campaign was characterized by a predominance of accumulation-mode particles, which accounted for 50.6% of the total N_{CN}, followed by the Aitken (46.8%) and nucleation modes (4.1%). Besides, the average N_{CCN} ranged from 902 to 2552 cm^{-3} at 0.2-0.7% SS. These values were generally consistent with the variability in N_{CN}: they were higher than those measured over the SCS in 2014, similar to the levels observed in 2018, and lower than the concentrations reported in 2021.(Atwood et al., 2017; Cai et al.,

https://doi.org/10.5194/egusphere-2026-4265
Preprint. Discussion started: 24 August 2026

2020; Ou et al., 2025)

The average NR-PM_1 concentration was 7.30 ± 4.24 μg m^{-3}, lower than the values measured in the South China Sea during the summers of 2018 (9.11 μg m^{-3}) and 2019 (10.65 μg m^{-3}), but higher than that observed in 2021 (3.76 μg m^{-3}).(Sun et al., 2023; Liang et al., 2021) Sulfate was the dominant component (42.8%), followed by organics (42.3%), ammonium (9.1%), nitrate (3.2%), and chloride (2.6%). The mean organic fraction exceeded those reported for the SCS in 2018, 2019, and 2021, and was more comparable to values observed in the Mediterranean region.(Mallet et al., 2019) Given that organic aerosols in the SCS are strongly influenced by anthropogenic emissions, the elevated organic contribution in this study suggests a greater impact of human activities relative to previous campaigns.

The average aerosol hygroscopicity parameter (κ) ranged from 0.34 to 0.43 at 0.2% - 0.7% SS, lower than the values observed over the SCS in the summer of 2021 (0.47-0.54 from 0.2% to 0.4% SS) but comparable to those reported in 2018 (0.38 at 0.18% SS).(Ou et al., 2025; Cai et al., 2020) The average bulk activation ratio (AR) varied from 0.28 to 0.72 across the same supersaturation range, remaining below the levels measured in both 2021 (0.37-0.87 at 0.2%-0.7% SS) and 2012 (0.47-0.85 at 0.15%-0.71% SS).(Ou et al., 2025; Atwood et al., 2017)

https://doi.org/10.5194/egusphere-2026-4265
Preprint. Discussion started: 24 August 2026

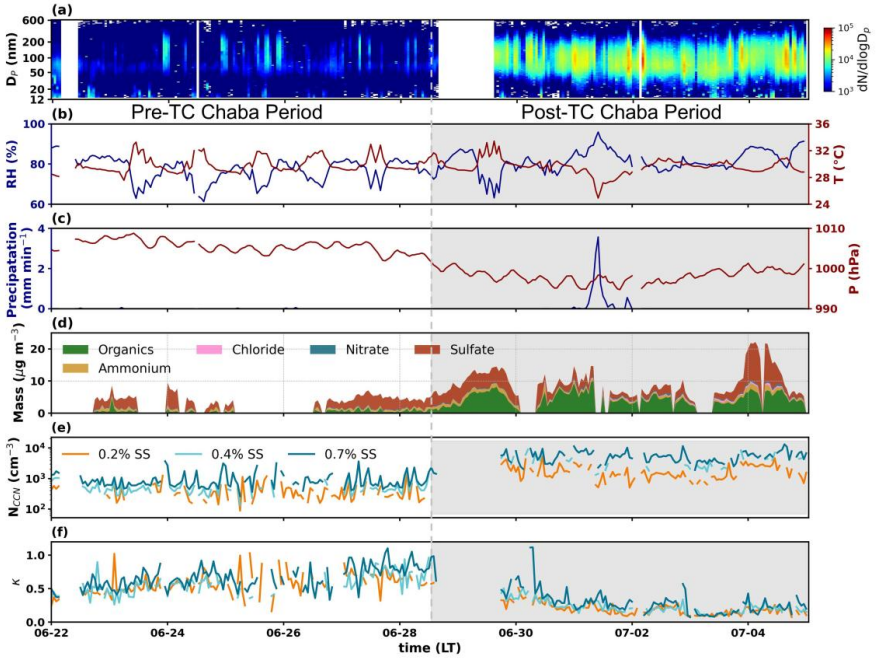

Figure 2 Timeseries of particle number size distribution (a), relative humidity (RH) and air temperature (T) (b), precipitation and pressure (P) (c), mass concentration of different aerosol composition (d), cloud condensation nuclei number concentration at different supersaturations (SS) (e), and aerosol hygroscopicity parameter (κ) at different SS.

3.2 Tropical cyclone "Chapa"-induced changes in aerosol physicochemical properties

Air masses over SCS changed markedly following the development of TC Chaba (Fig. S11). During pre-TC Chaba period, the region was dominated by local marine air masses, with a small fraction transported over Luzon Island. After the establishment of Chaba's circulation, air masses were primarily transported from the Indochina Peninsula. Correspondingly, the NR-PM_1 concentration increased from 4.51 to 8.84 μg m^{-3}. During the pre-TC Chaba period, NR-PM_1 was dominated by sulfate (67.3%), exhibiting a typical marine air-mass signature consistent with the backward-trajectory analysis. After the influence of TC Chaba, aerosol composition shifted substantially, with the organic aerosol (OA) fraction increasing from 14.6% to 44.9% and becoming the dominant aerosol component (Figs. 3 a and b). This increase was mainly driven by oxygenated organic aerosol (OOA), whose contribution rose from 9.8% to 38.5%. HOA and BBOA also increased but contributed much less than OOA, suggesting oxidation of these components during long-range transport.

https://doi.org/10.5194/egusphere-2026-4265
Preprint. Discussion started: 24 August 2026

Changes in the PNSD further illustrate the substantial impact of TC Chaba on aerosol physicochemical properties. The PNSD data were analyzed by fitting three characteristic modes: Nucleation, Aitken, and Accumulation. Subsequently, the effective diameter (D_{eff}) was also calculated from PNSD data. The detailed methodology for this procedure is described in Text S4. During post-TC Chaba period, the total aerosol number concentration increased markedly, driven primarily by enhancements in the aitken and accumulation modes (Figs. 3 c and d). The accumulation-mode contribution increased from 37.4% to 49.1%, indicating substantial aerosol aging and particle growth associated with long-range transport and secondary organic aerosol formation.

Besides, to investigate the drivers of OOA enhancement, we examined its relationship with meteorological and chemical parameters. During the post-TC Chaba period, OOA increased rapidly when relative humidity exceeded 75%, accompanied by an increase in oxidation state (Figs. 4 a and b). In addition, both OOA and total OA exhibited stronger positive correlations with Ox (O_3 + NO_2) during the post-TC period than during the pre-TC period, suggesting that Chaba-induced transport from the Indochina Peninsula strengthened the atmospheric oxidation capacity over the SCS and consequently promoted OA oxidation (Figs. 4 d and e). Together, these results indicate that both long-range transport and secondary formation contributed to the observed OOA enhancement. To further verify that this enhancement was not mainly caused by boundary layer evolution, OOA was normalized by ΔCO to account for boundary layer evolution. The diurnal variation of OOA/ΔCO exhibits a clear nighttime enhancement, indicating that the observed increase in OOA is not primarily driven by boundary layer effects, and further supporting a significant contribution of heterogeneous reactions to OOA formation. (Fig. S14).

Driven by the increased contribution of OA, particularly the enhanced fraction of OOA, κ decreased substantially during post-TC Chaba period. Specifically, κ ranged from 0.58-0.66 at 0.2%-0.7% SS before Chaba influence but declined sharply to 0.20-0.31 over the same SS range afterward (Figs. 3 c and d). During pre-TC Chaba period, the overall κ was comparable to values reported by Atwood et al., 2017 over the SCS, indicating a dominant marine air-mass influence. In contrast, during post-TC Chaba period, κ approached those measured in urban Guangzhou (Cai et al., 2018), further proving that Chaba-induced circulation changes facilitated the transport of anthropogenic aerosols from the Indochina

https://doi.org/10.5194/egusphere-2026-4265
Preprint. Discussion started: 24 August 2026

Peninsula into the SCS.

To further quantify the impact of OA on κ, we applied a linear parameterization between κ and the organic mass fraction (f_{OA}), as described by previous research (Huang et al., 2022; Bhattu et al., 2016). κ at 0.2% SS were used for this analysis because this lower SS better represents the hygroscopicity of larger particles and aligns more closely with the aerosol size range measured by the SV-ToF-ACSM (Ng et al., 2011). The resulting κ–f_{OA} relationships reveal a clear reduction in slope after the influence of Chaba under the dominance of Indochina air masses compared to marine conditions, which is consistent with the findings in the remote marine enviroments (Huang et al., 2022). Notably, the slope obtained under marine influence in this study is lower than that reported for remote marine, likely reflecting the relatively less pristine background conditions of the SCS.

Based on the κ–f_{OA} fits, κ_{OA} was defined as the κ value at f_{OA} = 1. The estimated κ_{OA} increase from 0.11 during pre-TC Chaba preiod to 0.15 during post-TC Chaba period, representing an approximately 27% increase (Figs. 4 c and f). The κ_{OA} is related to its oxidation state, with higher oxidation leading to greater hygroscopicity. During post-TC Chaba period, the fraction of OOA in total OA increased compared to the pre-TC Chaba period, thereby enhancing the overall oxidation level of OA, as further supported by the increase in the m/z 44-to-m/z 43 ratio from 4.78 to 6.36. Despite the increase in κ_{OA}, the bulk κ decreased significantly during post-TC Chaba period. This apparent discrepancy can be explained by the relatively low hygroscopicity of OA compared to inorganic components and its obviously higher fraction in total aerosol mass during post-TC Chaba period.

https://doi.org/10.5194/egusphere-2026-4265
Preprint. Discussion started: 24 August 2026

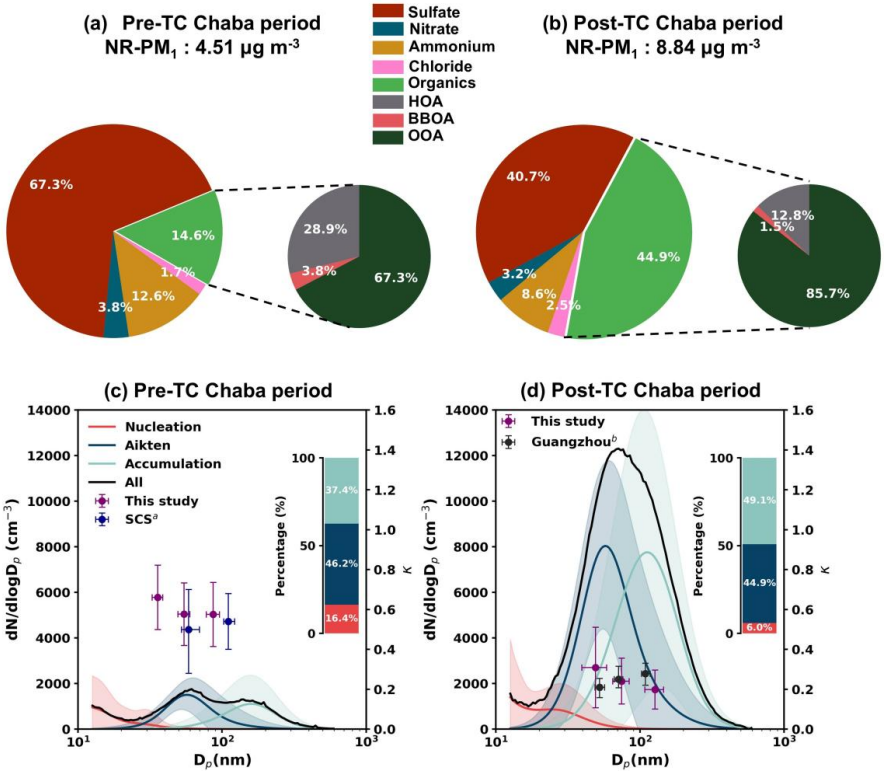

Figure 3. Aerosol composition mass concentration and fraction during pre-TC Chaba period (a) and post-TC Chaba period (b); Particle number size distribution, different particle mode fraction, activation diameter (D_{50}), and aerosol hygroscopicity parameter (κ) during pre-TC Chaba period (c) and post-TC Chaba period (d); In panels (c) and (d), the blue error bars represent the D_{50} and κ values derived in this study. The blue error bars (SCS[a]) indicate measurements reported by Atwood et al., 2017 over the SCS, and the black error bars (Guangzhou[b]) denote observations from Cai et al., 2018 conducted in the urban area of Guangzhou, China. The barplot presents the fraction of three particle modes.

https://doi.org/10.5194/egusphere-2026-4265
Preprint. Discussion started: 24 August 2026

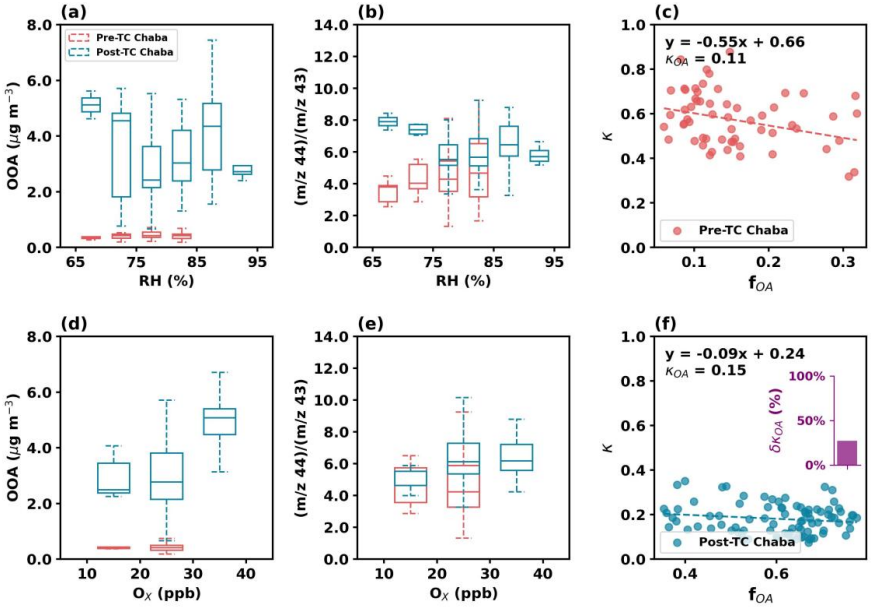

Figure 4. Comparison of Oxygenated Organic Aerosol (OOA) mass concentration and m/z 44/m/z 43 ratio as a function of Relative Humidity (RH) and O_x (O_3 + NO_2) during pre-TC Chaba and post-TC Chaba periods (a) OOA (μg m^{-3}) vs. RH (%); (b) m/z 44 / m/z 43 ratio vs. RH (%); (d) OOA (μg m-3) vs. O_x (ppb); (e) m/z 44 / m/z 43 ratio vs. O_x (ppb); (c) The linear parameterization between κ and the organic mass fraction (f_{OA}) during pre-TC Chaba period; (f) The linear parameterization between κ and the f_{OA} during post-TC Chaba period and the purple bar represents the decrease in κ_{OA}; The box plots illustrate the distribution of the data (whiskers: 10th and 90th percentiles; box: 25th, 50th (median), and 75th percentiles). Red boxes and circles represent data during pre-TC Chaba period, and blue boxes and circles represent data during post-TC Chaba period.

3.3 CCN activity response to aerosol property changes

Changes in the physicochemical properties of aerosols can influence their ability to activate into CCN which was also named CCN activity. It is primarily governed by two factors: particle size distribution and chemical composition. Chemical composition affects activation mainly by altering aerosol hygroscopicity (Petters and Kreidenweis, 2007). Here, we evaluate variations in CCN activity by examining changes in these two controlling factors. The bulk AR is used as the key metric to quantify CCN activity.

As described above, although the aerosol size distribution shifted toward larger particles because of the enhanced contribution from the accumulation mode, D_{eff} increased only slightly, from 92 nm to 96 nm

https://doi.org/10.5194/egusphere-2026-4265
Preprint. Discussion started: 24 August 2026

(~4%). In contrast, the decrease in aerosol hygroscopicity—driven by the substantial increase in organic aerosol fractions—was far more pronounced, which was described in previous section.

Considering the combined influence of these two factors, the bulk AR decreased from 0.33-0.80 at 0.2%-0.7% SS during pre-TC Chaba period to 0.24-0.73 during post-TC period (Fig. 5a). This indicates that the reduction in aerosol hygroscopicity exerted a stronger influence on CCN activation than the modest increase in particle size, making hygroscopicity the dominant driver of the observed decline in bulk AR. The decrease in bulk AR was also more pronounced at lower SS, consistent with the larger reduction in hygroscopicity for particles activated under low SS.

Although many previous studies have suggested that particle size distribution generally exerts a greater influence on CCN activity than aerosol hygroscopicity (Kuwata and Kondo, 2008; Dusek et al., 2006; Mcfiggans et al., 2006), our results demonstrate that hygroscopicity can become the controlling factor when changes in size distribution are relatively minor but decreases in hygroscopicity are substantial. The study in Western Pacific has shown that in clean oceanic environments, variations in aerosol hygroscopicity driven by marine biogenic emissions primarily regulate CCN activity (Kawana et al., 2022). Our findings further highlight that, under strong anthropogenic influence over marine regions, changes in OA fraction can influence aerosol hygroscopicity, thereby playing a crucial role in determining CCN activity.

https://doi.org/10.5194/egusphere-2026-4265
Preprint. Discussion started: 24 August 2026

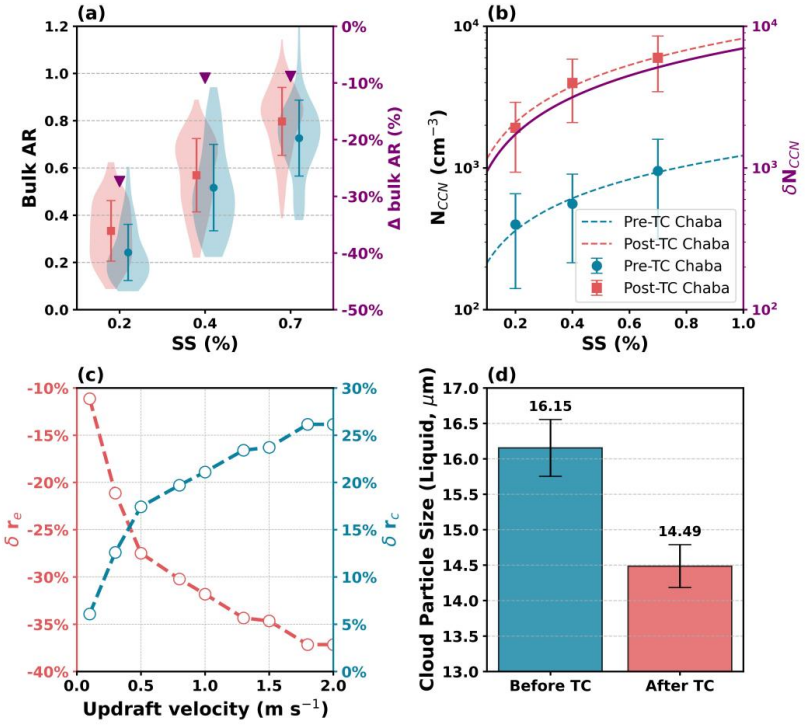

Figure 5. (a) The bulk activation ratio at different supersaturations (SS), the fitting result between the N_{CCN} and SS, and the change of N_{CCN} at different SS during pre-TC Chaba and post-TC Chaba periods; (b) The change of cloud effective radius (r_e) and critical radius (r_c) at different SS; (c) The average liquid cloud particle size from Modis data during pre-TC Chaba and post-TC Chaba period; It is noted that r_e and r_c refer to the Twomey effect and Albrecht effect, respectively. The spatial averaging domain for the MODIS data was defined as 12°N to 18°N latitude and 109°E to 112°E longitude. This entire region is located over the South China Sea and the ship's position was closed to the center.

3.4 Impacts on cloud microphysics and radiation effects

The influence of TC Chaba on aerosol physicochemical properties above points to a coherent chain of perturbations: the influx of anthropogenic aerosols from the Indochina Peninsula not only elevated particle concentrations but also substantially reduced aerosol hygroscopicity, which in turn suppressed CCN activity despite a modest increase in particle size. These shifts in aerosol properties could propagate further, with potential consequences for cloud microphysics over the SCS, which is discussed in this section. Cloud microphysics is influenced by two key mechanisms—the Twomey effect and the Albrecht effect. The Twomey effect describes how increases in N_{CCN} lead to higher cloud droplet number

https://doi.org/10.5194/egusphere-2026-4265
Preprint. Discussion started: 24 August 2026

concentrations and smaller droplet sizes, thereby enhancing cloud reflectivity and exerting a cooling radiative forcing (Twomey, 1959). In contrast, the Albrecht effect refers to the suppression of precipitation efficiency due to smaller droplet sizes, which reduces precipitation efficiency and extends cloud lifetime.(Albrecht, 1989) The cloud effective radius (r_e) and the critical diameter (r_c) represent the Twomey effect and Albrecht effect, respectively.

By analyzing the observed changes during pre-TC Chaba and post-TC Chaba periods, we assessed how shifts in aerosol properties modulated these two effects, providing insight into the microphysical and radiative implications of TC-driven aerosol perturbations over the SCS. Although the bulk AR decreased during post-TC Chaba period compared to pre-TC Chaba period, the marked increase in total N_{CN} resulted in a substantial enhancement of N_{CCN}. Across SS of 0.2–0.7%, N_{CCN} rose from 400–951cm^{-3} during pre-TC Chaba period to 1918–5981 cm^{-3} during post-TC Chaba period (Fig. 5b). In terms of change of N_{CCN}, the increase became more pronounced with rising SS during post-TC Chaba period, indicating that a larger number of smaller particles were activated as CCN.

The Pyrcel simulations linking the observed aerosol physicochemical properties to N_C are consistent with the observed N_{CCN}. Although the bulk AR decreased during post-TC Chaba period, the total activated particle number concentration increased due to the elevated N_{CN}. The simulation inputs are summarized in Table S2. Under the observed meteorological conditions and aerosol physicochemical properties, and within the prescribed updraft range, the critical maximum SS (S_{max}) was estimated to be ~0.03–0.28%. These relatively low SS suggest that aerosol activation occurred within an aerosol–updraft sensitive regime according to Reutter et al., 2009, rather than a purely aerosol-limited regime.(Reutter et al., 2009) This interpretation is supported by the pronounced dependence of N_C on both updraft velocity and aerosol concentration, as well as the reduction in S_{max} under enhanced aerosol conditions during the post-TC Chaba period (Table S2).

Based on the simulations, the r_e and r_c were derived for conditions during pre-TC Chaba and post-TC Chaba periods. As the updraft velocity increased from 0.1 to 2 m s^{-1}, r_e decreased by 11–37%, with a diminishing rate of decrease at higher updraft velocities. This pattern suggests that the influence of TC Chaba increased N_C while reducing droplet size, consistent with an enhancement in cloud albedo.

In contrast, r_c exhibited the opposite response. Across the same updraft range, r_c increased by 6–26%,

https://doi.org/10.5194/egusphere-2026-4265
Preprint. Discussion started: 24 August 2026

indicating reduced efficiency in the conversion of cloud droplets to raindrops during post-TC Chaba period, thereby probably suppressing precipitation formation.

The liquid cloud particle size retrieved from MODIS robustly validates our findings. Specifically, the liquid cloud particle size decreased from 16.15 μm during pre-TC Chaba period to 14.49 μm during post-TC Chaba period, an 11% reduction (Fig. 5d). This result is close to the simulation obtained under an assumed updraft velocity of 0.1 m s^{-1}, suggesting that the actual critical maximum supersaturation may be relatively low and primarily influences the activation of larger particles. However, discrepancies may still exist between the MODIS observations and the simulations constrained by in situ measurements. It primarily stems from two factors. First, the r_e calculation relies on changes in the N_C, which depends on uncertain updraft and dry adiabatic assumption. Secondly, the MODIS-retrieved liquid cloud particle size and r_e are not identical physical quantities. Nevertheless, the MODIS data confirms a definitive reduction in cloud droplet size. Considering the typical range of 0.1% to 0.3% SS for marine stratocumulus (Ditas et al., 2012), this result suggests that the changes in r_e and r_e were primarily driven by the influence of larger particles transported from the Indochina Peninsula following circulation changes induced by TC Chaba.

4. Discussions and Conclusions

Based on a shipborne observation during a TC event, our results show that TC-induced circulation changes can rapidly transform the marine boundary layer from a typical sulfate-dominated, highly hygroscopic marine background to a regime characterized by organic aerosol dominance, lower hygroscopicity, and substantially elevated aerosol concentrations associated with anthropogenic influence. During this transition, our results indicate that changes in hygroscopicity exert a stronger influence on CCN activity than changes in particle size distribution. This finding contrasts with results from other regions, where particle size distribution is often identified as the primary controlling factor for CCN activity and is as dominant control factor on aerosol activation in atmospheric models (Dusek et al., 2006). It suggests that models applied to marine regions periodically perturbed by continental outflow may systematically misrepresent N_{CCN} if hygroscopicity changes associated with OA loading are not adequately captured. Incorporating composition-dependent hygroscopicity parameterizations may

https://doi.org/10.5194/egusphere-2026-4265
Preprint. Discussion started: 24 August 2026

therefore be necessary to reduce biases in simulated N_{CCN} or N_C over such regions.

Besides, our results reflect implications for how TCs influence aerosol–cloud system. Our observations suggest that TC circulation can act as an efficient pump that episodically imports anthropogenic aerosol sources into pristine marine environments. This causes an increase in total aerosol population and then resulted in a higher number of activated cloud droplets. On the one hand, this leads to smaller droplet sizes, thereby enhancing cloud albedo and affecting the radiative balance. This is consistent with aircraft observations over the SCS showing that clouds influenced by industrial and biomass burning aerosols contain much higher concentrations of small droplets and fewer mid-sized droplets than clean marine clouds, in agreement with our results. On the other hand, the reduction in droplet size increases the critical radius required for the conversion of cloud droplets into raindrops, thereby suppressing warm rain formation and potentially influencing the regional hydrological cycle.

Recent studies suggest that although the frequency of TCs affecting the SCS exhibits complex variability (Huang et al., 2022), the intensity of both locally generated and westward-migrating TCs from the western North Pacific is increasing under climate change (Mei and Xie, 2016; Kossin et al., 2016). These TCs can repeatedly and rapidly transport anthropogenic aerosols from continental region into the marine region, establishing a anthropogenic influenced regime in their outer rainbands. These findings further suggest that TCs are not merely passive responders to climate change but also act as key amplifiers in ACI. Therefore, accurately projecting the future behavior of increasingly intense TCs over the SCS requires the explicit integration of these aerosol–microphysics–climate interactions into regional climate and weather prediction models.

Finally, it should be noted that this study is based on a single TC case and is constrained by the lack of direct in situ cloud microphysical measurements. Future work should expand to more TC events and incorporate direct observations of cloud microphysical parameters to better quantify the robustness and climatic relevance of the processes identified here. Given projected increases in TC intensity over the SCS,(Liu and Chan, 2020) such efforts are essential for improving our understanding of regional aerosol–cloud interactions and their implications for climate forcing and precipitation variability.

https://doi.org/10.5194/egusphere-2026-4265
Preprint. Discussion started: 24 August 2026

Data availability

The aerosol composition, meteorology, trace gas, cloud condensation nuclei, and aerosol hygroscopicity data from field measurements can be found on 10.6084/m9.figshare.32414736; The weekly GDAS1 (Global Data Assimilation System, 1° resolution) meteorological fields can be obtained from the NOAA Air Resources Laboratory (ARL) (https://www.ready.noaa.gov/gdas1.php); The MCD06COSP_D3_MODIS product can be found on http://doi.org/10.5067/MODIS/MCD06COSP_D3_MODIS.062

Author contributions

M. C. and H. W. designed the study and drafted the original manuscript. H. O. conducted data collection on board, performed the data analysis, and drafted the original manuscript. X. N., S. M., Q. S., and B. L. conducted data collection on board. T. D., J. S., and S. Z. contributed to improving the original manuscript. J. Z. designed the field measurement.

Competing interests

The contact author has declared that none of the authors has any competing interests.

Disclaimer

Copernicus Publications remain neutral with regard to jurisdictional claims made in the text, published maps, institutional affiliations, or any other geographical representation in this paper. While Copernicus Publications makes every effort to include appropriate place names, the final responsibility lies with the authors. Views expressed in the text are those of the authors and do not necessarily reflect the views of the publisher.

Financial support

This work was supported by National Natural Science Foundation of China (grant no. 42305123, 42175115), by Guangdong Basic and Applied Basic Research Foundation (grant no. 2024A1515030221), Science and Technology Projects in Guangzhou (grant no. 2025A04J4493), the Key Innovation Team of Guangdong Meteorological Bureau (grant no. GRMCTD202506-ZD06), Central Public interest

https://doi.org/10.5194/egusphere-2026-4265
Preprint. Discussion started: 24 August 2026

Scientific Institution Basal Research Fund of South China Institute of Environmental Sciences, MEE (grant no. PM-zx097-202506-214), and Basic Research Fund of the Institute of Tropical and Marine Meteorology (RDS202502)..

510

https://doi.org/10.5194/egusphere-2026-4265
Preprint. Discussion started: 24 August 2026

Reference

Albrecht, B. A.: Aerosols, cloud microphysics, and fractional cloudiness, Science, 245, 1227-1230, Https://doi.org/10.1126/science.245.4923.1227, 1989.

Atwood, S. A., Reid, J. S., Kreidenweis, S. M., et al.: Size-resolved aerosol and cloud condensation nuclei (CCN) properties in the remote marine South China Sea – Part 1: Observations and source classification, Atmos. Chem. Phys., 17, 1105-1123, Https://doi.org/10.5194/acp-17-1105-2017, 2017.

Bhatti, Y. A., Watson-Parris, D., Regayre, L. A., et al.: Uncertainty in aerosol effective radiative forcing from anthropogenic and natural aerosol parameters in ECHAM6.3-HAM2.3, Atmos. Chem. Phys., 26, 269-293, Https://doi.org/10.5194/acp-26-269-2026, 2026.

Bhattu, D., Tripathi, S. N., and Chakraborty, A.: Deriving aerosol hygroscopic mixing state from size-resolved CCN activity and HR-ToF-AMS measurements, Atmos Environ., 142, 57-70, Https://doi.org/10.1016/j.atmosenv.2016.07.032, 2016.

Black, M. L., Burpee, R. W., and Marks, F. D.: Vertical Motion Characteristics of Tropical Cyclones Determined with Airborne Doppler Radial Velocities, J. Atmos. Sci., 53, 1887-1909, Https://doi.org/10.1175/1520-0469(1996)053<1887:VMCOTC>2.0.CO;2, 1996.

Boucher, O. and Lohmann, U.: The sulfate-CCN-cloud albedo effect, Tellus B: Chemical and Physical Meteorology, 47, 281-300, Https://doi.org/10.3402/tellusb.v47i3.16048, 1995.

Cai, M., Liang, B., Sun, Q., et al.: Effects of continental emissions on cloud condensation nuclei (CCN) activity in the northern South China Sea during summertime 2018, Atmos. Chem. Phys., 20, 9153-9167, Https://doi.org/10.5194/acp-20-9153-2020, 2020.

Cai, M., Tan, H., Chan, C. K., et al.: The size-resolved cloud condensation nuclei (CCN) activity and its prediction based on aerosol hygroscopicity and composition in the Pearl Delta River (PRD) region during wintertime 2014, Atmos. Chem. Phys., 18, 16419-16437, Https://doi.org/10.5194/acp-18-16419-2018, 2018.

Chen, L., Li, Y., and Cheng, Z.: An overview of research and forecasting on rainfall associated with landfalling tropical cyclones, Adv. Atmos. Sci, 27, 967-976, Https://doi.org/10.1007/s00376-010-8171-y, 2010.

https://doi.org/10.5194/egusphere-2026-4265
Preprint. Discussion started: 24 August 2026

Chen, Y.-C., Christensen, M. W., Stephens, G. L., et al.: Satellite-based estimate of global aerosol–cloud radiative forcing by marine warm clouds, Nat. Geosci, 7, 643-646, Https://doi.org/10.1038/ngeo2214, 2014.

Ditas, F., Shaw, R. A., Siebert, H., et al.: Aerosols-cloud microphysics-thermodynamics-turbulence: evaluating supersaturation in a marine stratocumulus cloud, Atmos. Chem. Phys., 12, 2459-2468, Https://doi.org/10.5194/acp-12-2459-2012, 2012.

Dusek, U., Frank, G. P., Hildebrandt, L., et al.: Size Matters More Than Chemistry for Cloud-Nucleating Ability of Aerosol Particles, Science, 312, 1375-1378, Https://doi.org/10.1126/science.1125261, 2006.

Dusek, U., Frank, G. P., Hildebrandt, L., et al.: Size Matters More Than Chemistry for Cloud-Nucleating Ability of Aerosol Particles, 312, 1375-1378, Https://doi.org/doi:10.1126/science.1125261, 2006.

Geller, M., Biswas, S., and Sioutas, C.: Determination of Particle Effective Density in Urban Environments with a Differential Mobility Analyzer and Aerosol Particle Mass Analyzer, Aerosol Sci Tech, 40, 709-723, Https://doi.org/10.1080/02786820600803925, 2006.

Huang, P., Xu, J., and Liang, M.: Decadal variation in the frequency of tropical cyclones originating in the South China Sea and migrating from the western North Pacific, Front. Earth Sci, Volume 10 - 2022, Https://doi.org/10.3389/feart.2022.980220, 2022.

Huang, S., Wu, Z., Wang, Y., et al.: Aerosol Hygroscopicity and its Link to Chemical Composition in a Remote Marine Environment Based on Three Transatlantic Measurements, Environ Sci Technol, 56, 9613-9622, Https://doi.org/10.1021/acs.est.2c00785, 2022.

IPCC: Annex I: Observational Products [Trewin, B. (ed.)], in: Climate Change 2021: The Physical Science Basis. Contribution of Working Group I to the Sixth Assessment Report of the Intergovernmental Panel on Climate Change, edited by: Masson-Delmotte, V., Zhai, P., Pirani, A., Connors, S. L., Péan, C., Berger, S., Caud, N., Chen, Y., Goldfarb, L., Gomis, M. I., Huang, M., Leitzell, K., Lonnoy, E., Matthews, J. B. R., Maycock, T. K., Waterfield, T., Yelekçi, O., Yu, R., and Zhou, B., Cambridge University Press, Cambridge, United Kingdom and New York, NY, USA, 2061–2086, 10.1017/9781009157896.015, 2021.

https://doi.org/10.5194/egusphere-2026-4265
Preprint. Discussion started: 24 August 2026

Jose, S., Nair, V. S., and Babu, S. S.: Anthropogenic emissions from South Asia reverses the aero sol indirect effect over the northern Indian Ocean, Scientific Reports, 10, 18360, Https://doi.org/10.1038/s41598-020-74897-x, 2020.

Kawana, K., Miyazaki, Y., Omori, Y., et al.: Number-Size Distribution and CCN Activity of Atmospheric Aerosols in the Western North Pacific During Spring Pre-Bloom Period: Influences of Terrestrial and Marine Sources, J Geophys Res-Atmos, 127, e2022JD036690, Https://doi.org/10.1029/2022jd036690, 2022.

King, S. M., Butcher, A. C., Rosenoern, T., et al.: Investigating Primary Marine Aerosol Properties: CCN Activity of Sea Salt and Mixed Inorganic–Organic Particles, Environ Sci Technol, 46, 10405-10412, Https://doi.org/10.1021/es300574u, 2012.

Kossin, J. P., Emanuel, K. A., and Camargo, S. J.: Past and Projected Changes in Western North Pacific Tropical Cyclone Exposure, J. Clim, 29, 5725-5739, Https://doi.org/10.1175/JCLI-D-16-0076.1, 2016.

Kristensen, T. B., Müller, T., Kandler, K., et al.: Properties of cloud condensation nuclei (CCN) in the trade wind marine boundary layer of the western North Atlantic, Atmos. Chem. Phys., 16, 2675-2688, Https://doi.org/10.5194/acp-16-2675-2016, 2016.

Kuwata, M. and Kondo, Y.: Dependence of size-resolved CCN spectra on the mixing state of non volatile cores observed in Tokyo, J Geophys Res-Atmos, 113, Https://doi.org/10.1029/2007JD009761, 2008.

Lathem, T. L. and Nenes, A.: Water Vapor Depletion in the DMT Continuous-Flow CCN Chamber: Effects on Supersaturation and Droplet Growth, Aerosol Sci Tech, 45, 604-615, Https://doi.org/10.1080/02786826.2010.551146, 2011.

Liang, B., Cai, M., Sun, Q., et al.: Source apportionment of marine atmospheric aerosols in northern South China Sea during summertime 2018, Environ. Pollut., 289, 117948, Https://doi.org/10.1016/j.envpol.2021.117948, 2021.

Lin, X. and Huang, G.: Assessing Tropical Cyclone-Driven Aerosol Transport – A High-Resolution WRF-Chem Analysis of Major Hurricane Matthew and Implications for Future Climate Scenarios, Environ Sci Technol, 59, 9060-9071, Https://doi.org/10.1021/acs.est.5c02251, 2025.

https://doi.org/10.5194/egusphere-2026-4265
Preprint. Discussion started: 24 August 2026

595 Liu, K. S. and Chan, J. C. L.: Recent increase in extreme intensity of tropical cyclones making landfall in South China, Climate Dynamics, 55, 1059-1074, Https://doi.org/10.1007/s00382-020-05311-5, 2020.

Liu, L.-Y., Wei, G.-L., Wang, J.-Z., et al.: Anthropogenic Activities Have Contributed Moderately to Increased Inputs of Organic Materials in Marginal Seas off China, Environ Sci Technol, 47, 11414-11422, Https://doi.org/10.1021/es401751k, 2013.

Liu, Y., Daum, P. H., Guo, H., et al.: Dispersion bias, dispersion effect, and the aerosol–cloud conundrum, Environ. Res. Lett, 3, 045021, Https://doi.org/10.1088/1748-9326/3/4/045021, 2008.

Liu, Y., Daum, P. H., McGraw, R., et al.: Generalized threshold function accounting for effect of relative dispersion on threshold behavior of autoconversion process, Geophys Res Lett, 33, Https://doi.org/10.1029/2005GL025500, 2006.

Lu, M.-L. and Seinfeld, J. H.: Study of the Aerosol Indirect Effect by Large-Eddy Simulation of Marine Stratocumulus, Journal of the Atmospheric Sciences, 62, 3909-3932, Https://doi.org/10.1175/JAS3584.1, 2005.

Mallet, M. D., D'Anna, B., Même, A., et al.: Summertime surface PM1 aerosol composition and size by source region at the Lampedusa island in the central Mediterranean Sea, Atmos. Chem. Phys., 19, 11123-11142, Https://doi.org/10.5194/acp-19-11123-2019, 2019.

McFiggans, G., Artaxo, P., Baltensperger, U., et al.: The effect of physical and chemical aerosol properties on warm cloud droplet activation, Atmos. Chem. Phys., 6, 2593-2649, Https://doi.org/10.5194/acp-6-2593-2006, 2006.

615 Mei, W. and Xie, S.-P.: Intensification of landfalling typhoons over the northwest Pacific since the late 1970s, Nat. Geosci, 9, 753-757, Https://doi.org/10.1038/ngeo2792, 2016.

Meng, J. W., Yeung, M. C., Li, Y. J., et al.: Size-resolved cloud condensation nuclei (CCN) activity and closure analysis at the HKUST Supersite in Hong Kong, Atmos. Chem. Phys., 14, 10267-10282, Https://doi.org/10.5194/acp-14-10267-2014, 2014.

620 Miles, N. L., Verlinde, J., and Clothiaux, E. E.: Cloud Droplet Size Distributions in Low-Level Stratiform Clouds, Journal of the Atmospheric Sciences, 57, 295-311, Https://doi.org/https://doi.org/10.1175/1520-0469(2000)057<0295:CDSDIL>2.0.CO;2, 2000.

https://doi.org/10.5194/egusphere-2026-4265
Preprint. Discussion started: 24 August 2026

Moore, R. H., Nenes, A., and Medina, J.: Scanning Mobility CCN Analysis—A Method for Fast Measurements of Size-Resolved CCN Distributions and Activation Kinetics, Aerosol Sci Tech, 44, 861-871, Https://doi.org/10.1080/02786826.2010.498715, 2010.

Ng, N. L., Canagaratna, M. R., Jimenez, J. L., et al.: Real-Time Methods for Estimating Organic Component Mass Concentrations from Aerosol Mass Spectrometer Data, Environ Sci Technol, 45, 910-916, Https://doi.org/10.1021/es102951k, 2011.

Ng, N. L., Herndon, S. C., Trimborn, A., et al.: An Aerosol Chemical Speciation Monitor (ACSM) for Routine Monitoring of the Composition and Mass Concentrations of Ambient Aerosol, Aeros ol Sci Tech, 45, 780-794, Https://doi.org/10.1080/02786826.2011.560211, 2011.

Ou, H., Cai, M., Zhang, Y., et al.: Measurement report: Cloud condensation nuclei (CCN) activity in the South China Sea from shipborne observations during the summer and winter of 2021 – sea sonal variation and anthropogenic influence, Atmos. Chem. Phys., 25, 2495-2513, Https://doi.org/1 0.5194/acp-25-2495-2025, 2025.

Petters, M. D. and Kreidenweis, S. M.: A single parameter representation of hygroscopic growth a nd cloud condensation nucleus activity, Atmos. Chem. Phys., 7, 1961-1971, Https://doi.org/10.5194 /acp-7-1961-2007, 2007.

Qin, Y., Wang, H., Wang, Y., et al.: Wildfires in Southeast Asia pollute the atmosphere in the nort hern South China Sea, Science Bulletin, 69, 1011-1015, Https://doi.org/10.1016/j.scib.2024.02.026, 2024.

Qiu, S., Zheng, X., Painemal, D., et al.: Daytime variation in the aerosol indirect effect for warm marine boundary layer clouds in the eastern North Atlantic, Atmos. Chem. Phys., 24, 2913-2935, Https://doi.org/10.5194/acp-24-2913-2024, 2024.

Quaas, J., Boucher, O., and Bréon, F. M.: Aerosol indirect effects in POLDER satellite data and t he Laboratoire de Météorologie Dynamique–Zoom (LMDZ) general circulation model, J Geophys Res-Atmos, 109, Https://doi.org/10.1029/2003JD004317, 2004.

Regayre, L. A., Schmale, J., Johnson, J. S., et al.: The value of remote marine aerosol measureme nts for constraining radiative forcing uncertainty, Atmos. Chem. Phys., 20, 10063-10072, Https://d oi.org/10.5194/acp-20-10063-2020, 2020.

https://doi.org/10.5194/egusphere-2026-4265
Preprint. Discussion started: 24 August 2026

Reutter, P., Su, H., Trentmann, J., et al.: Aerosol- and updraft-limited regimes of cloud droplet for mation: influence of particle number, size and hygroscopicity on the activation of cloud condensati on nuclei (CCN), Atmos. Chem. Phys., 9, 7067-7080, Https://doi.org/10.5194/acp-9-7067-2009, 20 09.

Rotstayn, L. D. and Liu, Y.: Cloud droplet spectral dispersion and the indirect aerosol effect: Com parison of two treatments in a GCM, Geophys Res Lett, 36, Https://doi.org/10.1029/2009GL03821 6, 2009.

Seifert, A. and Beheng, K. D.: A two-moment cloud microphysics parameterization for mixed-phas e clouds. Part 1: Model description, Meteorol. Atmos. Phys, 92, 45-66, Https://doi.org/10.1007/s00 703-005-0112-4, 2006.

Shao, M., Yang, J., Wang, J., et al.: Co-Occurrence of Surface O3, PM2.5 Pollution, and Tropical Cyclones in China, J Geophys Res-Atmos, 127, e2021JD036310, Https://doi.org/10.1029/2021JD03 6310, 2022.

Sun, Q., Liang, B., Cai, M., et al.: Cruise observation of the marine atmosphere and ship emissio ns in South China Sea: Aerosol composition, sources, and the aging process, Environ. Pollut., 316, 120539, Https://doi.org/10.1016/j.envpol.2022.120539, 2023.

Twomey, S.: The nuclei of natural cloud formation part II: The supersaturation in natural clouds a nd the variation of cloud droplet concentration, Pure Appl. Geophys, 43, 243-249, Https://doi.org/1 0.1007/BF01993560, 1959.

Wall, C. J., Storelvmo, T., and Possner, A.: Global observations of aerosol indirect effects from m arine liquid clouds, Atmos. Chem. Phys., 23, 13125-13141, Https://doi.org/10.5194/acp-23-13125-2 023, 2023.

Wang, G., Su, J., Ding, Y., et al.: Tropical cyclone genesis over the south China sea, Journal of Marine Systems, 68, 318-326, Https://doi.org/10.1016/j.jmarsys.2006.12.002, 2007.

Wang, H., Rasch, P. J., and Feingold, G.: Manipulating marine stratocumulus cloud amount and al bedo: a process-modelling study of aerosol-cloud-precipitation interactions in response to injection of cloud condensation nuclei, Atmos. Chem. Phys., 11, 4237-4249, Https://doi.org/10.5194/acp-11-4237-2011, 2011.

https://doi.org/10.5194/egusphere-2026-4265
Preprint. Discussion started: 24 August 2026

Wang, N., Huang, X., Xu, J., et al.: Typhoon-boosted biogenic emission aggravates cross-regional ozone pollution in China, Sci. Adv, 8, eabl6166, Https://doi.org/10.1126/sciadv.abl6166, 2022.

Wang, S., Murakami, H., and Cooke, W. F.: Anthropogenic forcing changes coastal tropical cyclone frequency, npj Clim. Atmos. Sci., 6, 187, Https://doi.org/10.1038/s41612-023-00516-x, 2023.

Wang, X., Wang, C., Han, G., et al.: Effects of tropical cyclones on large-scale circulation and ocean heat transport in the South China Sea, Climate Dynamics, 43, 3351-3366, Https://doi.org/10.1007/s00382-014-2109-5, 2014.

Wang, Y., Lee, K.-H., Lin, Y., et al.: Distinct effects of anthropogenic aerosols on tropical cyclones, Nat. Clim. Change, 4, 368-373, Https://doi.org/10.1038/nclimate2144, 2014.

Wang, Y. Q.: MeteoInfo: GIS software for meteorological data visualization and analysis, Meteorol. Appl, 21, 360-368, Https://doi.org/10.1002/met.1345, 2014.

Webb, M. J., Andrews, T., Bodas-Salcedo, A., et al.: The Cloud Feedback Model Intercomparison Project (CFMIP) contribution to CMIP6, Geosci. Model Dev., 10, 359-384, Https://doi.org/10.5194/gmd-10-359-2017, 2017.